

Lepton Mixing from a Lattice Flavon Model: A Two-Branch Octant- δ Prediction

Vernon Barger¹

¹*Department of Physics, University of Wisconsin–Madison, Madison, Wisconsin 53706, USA*
(Dated: March 6, 2026)

We extend the single-flavon B -lattice Froggatt–Nielsen (FN) framework—previously successful for quark masses and Cabibbo-Kobayashi-Maskawa (CKM) mixing—to the lepton sector. The same B -lattice power structure ($\epsilon \equiv 1/B \simeq 0.19$) generates charged-lepton mass hierarchies and a normal-ordered neutrino spectrum; large neutrino mixing angles require an additional approximate mu–tau symmetry, broken at $\mathcal{O}(\epsilon)$ to generate a nonzero reactor angle and CP-violating phase.

The Pontecorvo-Maki-Nakagawa-Sakata (PMNS) matrix factorizes as $U_{\text{PMNS}} = U_e^\dagger U_\nu$, with near-tribimaximal U_ν corrected by small charged-lepton rotations whose phases are naturally aligned by the single-flavon origin of the Yukawa textures. This alignment produces a two-branch prediction in the (θ_{23}, δ) plane: a lower-octant solution with $\theta_{23} \approx 43^\circ$, $\delta \approx 286^\circ$, and an upper-octant solution with $\theta_{23} \approx 46^\circ$, $\delta \approx 304^\circ$. The lower octant is favored by a $\sim 4:1$ theoretical prior. The Jarlskog invariant $J_{\text{CP}} \simeq -0.027$ is nearly branch-independent; only precision measurements of the atmospheric octant and Dirac phase at DUNE, Hyper-Kamiokande, IceCube, and JUNO can distinguish the two solutions.

I. INTRODUCTION

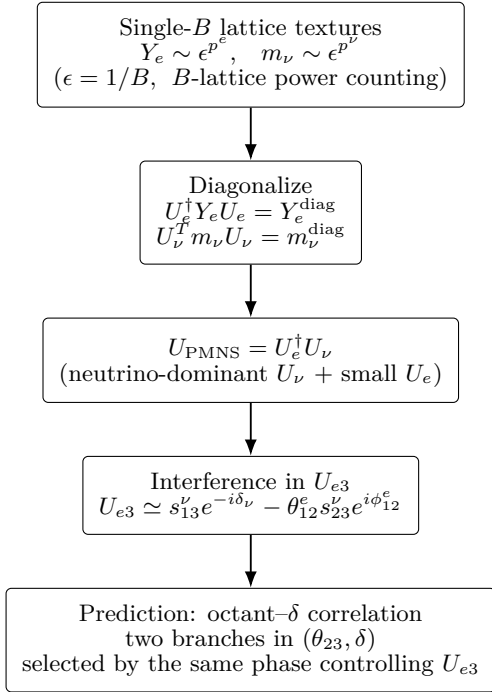


FIG. 1. Schematic logic of the single- B lattice-flavon lepton analysis. Neutrino-dominant mixing corrected by B -lattice charged-lepton rotations produces an interference-controlled reactor element U_{e3} , implying a predictive two-branch octant- δ structure.

The Froggatt–Nielsen mechanism [1–3] offers a natural framework for addressing fermion mass hierarchies through a single expansion parameter. In this work we develop the lepton sector of the lattice-flavon (“ninth”) implementation [4–6], in which fermion mass matrices

are organized by powers of $\epsilon = 1/B$, with $B = 75/14$. The same single- B structure that successfully accounts for quark masses and CKM mixing [7, 8] is applied here to charged leptons and neutrinos, supplemented in the neutrino sector by an approximate mu–tau symmetry that produces the large atmospheric and solar angles.

The observed pattern of lepton mixing—large solar and atmospheric angles together with a comparatively small but nonzero reactor angle and a sizable Dirac CP phase [9]—provides a rich testing ground for this framework.

Lepton mixing factorizes as [10, 11]

$$U_{\text{PMNS}} = U_e^\dagger U_\nu, \quad (1)$$

so that the observed angles and phases arise from controlled interference between neutrino-dominant mixing and small charged-lepton rotations fixed by B -lattice power counting. This structure leads to a predictive linkage: the same interference that generates U_{e3} correlates the atmospheric-octant selection with the displacement of the Dirac phase δ (Fig. 1).

We derive analytic diagonalization formulas, perform representative coefficient scans consistent with NuFIT 6.0 [9] normal ordering, and present a compact analytic relation encoding the two-branch octant- δ structure. The resulting correlation provides a sharp and experimentally testable signature of the single- B lattice-flavon organizing principle at DUNE [12], Hyper-Kamiokande [13], IceCube [14], and JUNO [15].

II. FLAVON LATTICE AND MESSENGER FRAMEWORK

The flavor structure is generated by a single Froggatt–Nielsen flavon field [1–3] Φ with $\langle \Phi \rangle / \Lambda = 1/B \equiv \epsilon$. Effective Yukawa operators arise from integrating out

heavy vectorlike messenger chains, producing suppression factors of the form

$$Y_{ij} \sim c_{ij} \epsilon^{p_{ij}} e^{i\phi_{ij}}, \quad (2)$$

where p_{ij} are rational lattice exponents determined by messenger insertions, $c_{ij} = \mathcal{O}(1)$ coefficients, and ϕ_{ij} are physical phases.

Exponent Structure

In the charged-lepton sector, the additive charge rule

$$p_{ij}^e = p_{L_i}^e + p_{R_j}^e \quad (3)$$

generates hierarchical masses controlled by the lattice exponents, with the specific charge assignments detailed in Sec. IV.

The neutrino mass matrix (for normal ordering) follows

$$m_1 : m_2 : m_3 \sim B^{-2} : B^{-1} : 1. \quad (4)$$

Phase Structure

Physical CP violation arises from relative phases between entries. After field redefinitions removing unphysical phases, the remaining Dirac phase appears through interference of left-handed rotations:

$$U_{\text{PMNS}} = U_e^\dagger U_\nu. \quad (5)$$

In the Fritzsch–Xing (FX) convention [16] adopted here for the lepton sector, the Dirac phase is associated with the U_{e3} element (in direct analogy with the CKM choice where the FX phase resides in V_{us}). Writing the FX parameterization schematically as

$$U_{\text{PMNS}}^{(\text{FX})} = R_{12}^T(\theta_\ell) P_\phi R_{23}(\theta) R_{12}(\theta_\nu), \quad (6)$$

$$P_\phi \equiv \text{diag}(1, e^{i\phi_{\text{FX}}}, 1).$$

one sees explicitly that the leptonic Jarlskog invariant [17] takes the form

$$J_{\text{CP}} = s_\ell c_\ell s_\nu c_\nu s^2 c \sin \phi_{\text{FX}}, \quad (7)$$

Relation to the Particle Data Group (PDG) phase [18]. Because the Jarlskog invariant is basis independent, one may equate the FX and PDG forms,

$$J_{\text{CP}}^{(\text{FX})} = J_{\text{CP}}^{(\text{PDG})}, \quad (8)$$

where in the PDG convention

$$J_{\text{CP}}^{(\text{PDG})} = s_{12} c_{12} s_{23} c_{23} s_{13} c_{13}^2 \sin \delta_{\text{PDG}}. \quad (9)$$

Hence

$$s_\ell c_\ell s_\nu c_\nu s^2 c \sin \phi_{\text{FX}} = s_{12} c_{12} s_{23} c_{23} s_{13} c_{13}^2 \sin \delta_{\text{PDG}}. \quad (10)$$

The invariant physical quantity is J_{CP} ; the parameter phases ϕ_{FX} and δ_{PDG} coincide only when the angle definitions match exactly.

Diagonalization

Given a Yukawa matrix Y , biunitary diagonalization yields

$$U_L^\dagger Y U_R = Y^{\text{diag}}. \quad (11)$$

Remark. While only the left-handed rotation matrices U_L enter directly into the observable PMNS matrix, the right-handed matrices U_R and their associated angles contribute to the diagonalization of the Yukawa operator and therefore enter the physical charged-lepton mass eigenvalues. In hierarchical B -lattice textures the scaling of m_ℓ depends on the combined left- and right-handed exponents, even though U_R drops out of the low-energy mixing matrix.

Illustrative 2×2 example. To see how the additive charge rule translates into mixing angles, consider a 2×2 charged-lepton sub-block with lattice exponents,

$$p = \begin{pmatrix} p_{L_1} + p_{R_1} & p_{L_1} + p_{R_2} \\ p_{L_2} + p_{R_1} & p_{L_2} + p_{R_2} \end{pmatrix}, \quad (12)$$

$$Y \sim \begin{pmatrix} B^{-p_{11}/9} & B^{-p_{12}/9} \\ B^{-p_{21}/9} & B^{-p_{22}/9} \end{pmatrix}. \quad (13)$$

If $p_{22} < p_{12}$ and $p_{22} < p_{21}$, the dominant entry is Y_{22} and the left- and right-handed mixing angles obtained by biunitary diagonalization scale as

$$\theta_{12}^L \sim \frac{Y_{12}}{Y_{22}} \sim B^{-(p_{12}-p_{22})/9}, \quad (14)$$

$$\theta_{12}^R \sim \frac{Y_{21}}{Y_{22}} \sim B^{-(p_{21}-p_{22})/9}.$$

Thus the same additive rule that fixes the diagonal suppressions (and hence mass ratios) automatically controls the rotation angles, with generally distinct left- and right-handed hierarchies when $p_{12} \neq p_{21}$. The observable mixing from this block is governed by the column suppression (left rotation), and in general

$$\theta_{ij}^L \sim B^{-(p_{ij}-p_{jj})/9}, \quad (15)$$

ensuring that off-diagonal elements are suppressed relative to diagonal entries. Large leptonic mixing emerges when the neutrino sector provides comparable rotations that interfere with the small charged-lepton rotations.

Tribimaximal limit

The FX parameterization makes the role of the charged-lepton rotation θ_ℓ especially transparent. Setting $\theta_\ell = 0$ (i.e. switching off charged-lepton mixing) gives $U_{e3} = -s_\ell e^{i\phi_{\text{FX}}} \sin \theta = 0$, and the PMNS matrix reduces to

$$U_{\text{PMNS}}^{(\theta_\ell=0)} = \begin{pmatrix} c_\nu & s_\nu & 0 \\ -e^{i\phi} c s_\nu & e^{i\phi} c c_\nu & e^{i\phi} s \\ s s_\nu & -s c_\nu & c \end{pmatrix}, \quad (16)$$

where $c \equiv \cos\theta$, $s \equiv \sin\theta$, and the shorthand c_ν, s_ν stands for $\cos\theta_\nu, \sin\theta_\nu$. Substituting the tribimaximal (TBM) values [19] $\theta_\nu = \arctan(1/\sqrt{2}) \approx 35.26^\circ$ and $\theta = \pi/4$ reproduces the familiar TBM pattern

$$|U_{\text{TBM}}| = \begin{pmatrix} \sqrt{2/3} & 1/\sqrt{3} & 0 \\ 1/\sqrt{6} & 1/\sqrt{3} & 1/\sqrt{2} \\ 1/\sqrt{6} & 1/\sqrt{3} & 1/\sqrt{2} \end{pmatrix}. \quad (17)$$

In this limit the phase ϕ_{FX} is unobservable: it multiplies the entire second row and can be absorbed by a muon-field redefinition, giving $J_{\text{CP}} = s_\ell c_\ell \cdots \sin\phi_{\text{FX}} = 0$.

Three consequences are immediate: (i) exact TBM resides entirely in U_ν , parameterized by (θ_ν, θ) alone; (ii) all departures from TBM—nonzero θ_{13} , atmospheric octant displacement, and the Dirac CP phase—switch on together when $\theta_\ell \neq 0$; (iii) since the B -lattice fixes $\theta_\ell \sim \epsilon \approx 0.19$ through the charged-lepton hierarchy, the same small parameter that controls m_e/m_μ simultaneously determines U_{e3} , the octant shift, and δ , producing the predictive two-branch correlation analyzed in Sec. XI.

III. SINGLE- B FRAMEWORK

We work with

$$\epsilon \equiv \frac{1}{B}, \quad B = \frac{75}{14} \simeq 5.357, \quad \epsilon \simeq 0.1867. \quad (18)$$

Lepton mixing factorizes as in Eq. (5).

IV. CHARGED-LEPTON SECTOR: ANALYTIC EIGENVECTORS

We adopt the symmetric texture

$$p^e = \frac{1}{18} \begin{pmatrix} 87 & 64 & 40 \\ 64 & 30 & 36 \\ 40 & 36 & 0 \end{pmatrix}, \quad (Y_e)_{ij} = c_{ij}^e \epsilon^{p_{ij}^e}. \quad (19)$$

Remark. The symmetric texture above departs from strict charge additivity $p_{ij}^e = p_{L_i}^e + p_{R_j}^e$ in the $(2, 3)$ sector, where the off-diagonal suppression ϵ^2 is stronger than the additive rule would predict ($\epsilon^{1/2}$). Physically, this additional suppression of the μ - τ charged-lepton rotation can be attributed to a selection rule or alignment in the messenger sector that forbids the leading messenger chain connecting the second and third generations. This ensures that the charged-lepton contribution to atmospheric mixing remains a perturbative correction to the neutrino-dominant structure.

This texture also implies effective lepton-doublet charges $Q(L_i)^{\text{eff}} \simeq (1, 0, 0)$, differing from the Weinberg-operator [20] assignments $Q(L_i) = (1, \frac{1}{2}, 0)$ adopted in the companion paper [5]. The companion paper uses the additive rule $p_{ij}^e = Q(L_i) + Q(L_j)$ to construct the

neutrino exponent texture, yielding a hierarchical matrix with $p_{22}^e = 1$, $p_{23}^e = \frac{1}{2}$, $p_{33}^e = 0$. That assignment correctly reproduces the neutrino mass eigenvalue hierarchy $m_1 : m_2 : m_3 \sim \epsilon^2 : \epsilon : 1$, which is the only neutrino observable analyzed there. However, the hierarchical 23 block does not by itself produce the large atmospheric and solar mixing angles observed in the PMNS matrix; these require the flat $\mathcal{O}(1)$ structure of Eq. (28) together with an approximate mu-tau symmetry, as developed in Sec. VB below. The two treatments are therefore complementary: the companion paper establishes the B -lattice mass scaling common to both, while the present paper introduces the additional symmetry structure needed for the PMNS mixing pattern.

Non-uniqueness and minimal symmetric completion. The left-handed power counting is controlled by column differences $p_{ij}^{eL} \equiv p_{ij}^e - p_{jj}^e$ (since $(U_{eL})_{ij} \sim \epsilon^{p_{ij}^e - p_{jj}^e}$). Therefore, for a fixed p^{eL} the most general (possibly asymmetric) texture is

$$p_{ij}^e = p_{ij}^{eL} + d_j, \quad d_j \equiv p_{jj}^e, \quad (20)$$

i.e. the three diagonal exponents d_j parameterize the remaining freedom and determine the right-handed differences $p_{ij}^{eR} = p_{ij}^e - p_{ii}^e = p_{ij}^{eL} + d_j - d_i$. Imposing the additional condition $p^e = p^{eT}$ fixes the diagonal differences uniquely (up to an overall shift) via $d_j - d_i = p_{ji}^{eL} - p_{ij}^{eL}$, yielding the symmetric matrix used in this paper as the minimal symmetric completion of the chosen U_{eL} power counting.

The diagonal entries of Eq. (19)— $p_{11}^e = \frac{29}{6}$, $p_{22}^e = \frac{5}{3}$, $p_{33}^e = 0$ —fix the charged-lepton mass hierarchy:

$$m_e : m_\mu : m_\tau \sim c_e \epsilon^{29/6} : c_\mu \epsilon^{5/3} : 1, \quad (21)$$

where $c_e, c_\mu = \mathcal{O}(1)$. Using $\overline{\text{MS}}$ masses at M_Z [5], $\epsilon^{29/6} \simeq 3.0 \times 10^{-4}$ and $\epsilon^{5/3} \simeq 6.1 \times 10^{-2}$, giving $c_e \simeq 0.93$ and $c_\mu \simeq 0.97$. The muon coefficient c_μ is fixed by the $\mathcal{O}(1)$ entries in the $(2, 2)$ and $(2, 3)$ sub-block of the Yukawa matrix; its proximity to unity is nontrivial, since the off-diagonal entry $(Y_e)_{23} \sim \epsilon^2$ is only mildly suppressed relative to $(Y_e)_{22} \sim \epsilon^{5/3}$ and contributes an $\mathcal{O}(\epsilon^{1/3}) \approx 57\%$ correction to the naive diagonal estimate of m_μ .

To leading nontrivial order, the orthonormal eigenvectors of $Y_e Y_e^\dagger$ are

$$v_\tau \simeq (0, 0, 1)^T + \mathcal{O}(\epsilon^2), \quad (22)$$

$$v_\mu \simeq (0, 1, -\epsilon^2)^T + \mathcal{O}(\epsilon^{17/9}), \quad (23)$$

$$v_e \simeq (1, -\epsilon^{17/9}, -\epsilon^{20/9})^T + \mathcal{O}(\epsilon^2). \quad (24)$$

Thus

$$U_e \simeq \begin{pmatrix} 1 & \epsilon^{17/9} & \epsilon^{20/9} \\ -\epsilon^{17/9} & 1 & \epsilon^2 \\ -\epsilon^{20/9} & -\epsilon^2 & 1 \end{pmatrix}. \quad (25)$$

V. NEUTRINO SECTOR: MASS TEXTURE AND NEAR-TBM MIXING

A. B -lattice mass hierarchy

For normal ordering the B -lattice assigns

$$m_3 : m_2 : m_1 \sim 1 : \epsilon : \epsilon^2, \quad (26)$$

giving $m_3 \simeq 50$ meV, $m_2 \simeq 9$ meV, $m_1 \simeq 2$ meV. This hierarchy is a direct consequence of the B -lattice power counting and holds independently of the $\mathcal{O}(1)$ structure of the neutrino mass matrix.

B. Mu–tau symmetry and the $\mathcal{O}(1)$ structure

The B -lattice hierarchy alone does not determine the neutrino mixing pattern. Large atmospheric and solar angles require additional structure in the $\mathcal{O}(1)$ coefficients of the effective mass matrix

$$(m_\nu)_{ij} = c_{ij}^\nu \epsilon^{p_{ij}^\nu} m_0, \quad (27)$$

where m_0 sets the overall neutrino mass scale. The FN charge assignment $p_{L_1}^\nu \gg p_{L_2}^\nu = p_{L_3}^\nu$ produces the exponent structure

$$p^\nu = \frac{1}{9} \begin{pmatrix} 9 & 9 & 9 \\ 9 & 0 & 0 \\ 9 & 0 & 0 \end{pmatrix}, \quad (28)$$

which suppresses the first-generation couplings by $\mathcal{O}(\epsilon)$ relative to the 23 block. However, the $\mathcal{O}(1)$ entries in the 23 block must satisfy approximate *mu–tau symmetry* [21–23]:

$$c_{22}^\nu \simeq c_{33}^\nu, \quad c_{12}^\nu \simeq c_{13}^\nu, \quad (29)$$

together with a near-maximal ratio $c_{23}^\nu/c_{22}^\nu \simeq -1$.

The minimal symmetry enforcing Eq. (29) is a $Z_2^{\mu\tau}$ exchange under which $L_\mu \leftrightarrow L_\tau$ (equivalently, $\nu_\mu \leftrightarrow \nu_\tau$). Larger discrete groups such as A_4 or S_4 , which contain the mu–tau reflection as a subgroup, also produce this structure and additionally constrain the solar angle toward its tribimaximal value [24, 25]. With this input, the leading-order effective mass matrix takes the form

$$\frac{m_\nu}{m_3} \simeq \begin{pmatrix} \mathcal{O}(\epsilon) & \mathcal{O}(\epsilon) & \mathcal{O}(\epsilon) \\ \mathcal{O}(\epsilon) & \frac{1}{2} & -\frac{1}{2} \\ \mathcal{O}(\epsilon) & -\frac{1}{2} & \frac{1}{2} \end{pmatrix}, \quad (30)$$

whose 23 block has eigenvalues 0 and 1 (in units of m_3), giving maximal atmospheric mixing, while the first-generation entries mix via the m_2 eigenvalue to produce a near-tribimaximal solar angle [19].

C. $\mathcal{O}(\epsilon)$ mu–tau breaking and θ_{13}^ν

Exact mu–tau symmetry forces $\theta_{13} = 0$, which is excluded by experiment. The required $\theta_{13}^\nu \sim \epsilon \approx 0.15$ is generated by $\mathcal{O}(\epsilon)$ breaking of the $Z_2^{\mu\tau}$,

$$\delta(m_\nu)_{12} - \delta(m_\nu)_{13} \sim \epsilon m_3, \quad (31)$$

which splits the first row and introduces a nonzero reactor angle together with a CP-violating neutrino-sector phase δ_ν . In the B -lattice picture this breaking arises naturally: the FN charges of the second and third generations differ in the charged-lepton sector ($p_{L_2}^e \neq p_{L_3}^e$), and this difference feeds into the neutrino texture at $\mathcal{O}(\epsilon)$ through higher-order operators or renormalization-group running below the seesaw scale [26–29].

D. Resulting U_ν and summary

The combined hierarchy plus mu–tau structure yields a near-tribimaximal diagonalization matrix

$$U_\nu \simeq \begin{pmatrix} \frac{2}{\sqrt{6}} & \frac{1}{\sqrt{3}} & \mathcal{O}(\epsilon) \\ -\frac{1}{\sqrt{6}} & \frac{1}{\sqrt{3}} & \frac{1}{\sqrt{2}} \\ -\frac{1}{\sqrt{6}} & \frac{1}{\sqrt{3}} & -\frac{1}{\sqrt{2}} \end{pmatrix}, \quad (32)$$

whose columns are the eigenvectors

$$u_3 \simeq \frac{1}{\sqrt{2}}(0, 1, -1)^T, \quad (33)$$

$$u_2 \simeq \frac{1}{\sqrt{3}}(1, 1, 1)^T, \quad (34)$$

$$u_1 \simeq \frac{1}{\sqrt{6}}(2, -1, -1)^T, \quad (35)$$

up to $\mathcal{O}(\epsilon)$ corrections that generate $\theta_{13}^\nu \sim \epsilon$.

Thus the neutrino sector draws on two distinct ingredients: the B -lattice hierarchy for the mass eigenvalues and the first-generation suppression, and a mu–tau exchange symmetry ($Z_2^{\mu\tau}$, A_4 , or S_4) for the $\mathcal{O}(1)$ structure of the 23 block. The charged-lepton sector, by contrast, requires only FN power counting. The interplay between these two sectors—neutrino-dominant large angles corrected by small charged-lepton rotations—is the mechanism that produces the predictive octant– δ correlation analyzed in Sec. XI.

VI. NUMERICAL DIAGONALIZATION AND PMNS MATRIX

We adopt a representative benchmark in the NO-I region identified by the scan (Sec. XI): neutrino-sector phase $\delta_\nu = 295^\circ$, $\theta_{13}^\nu = 0.15$ rad, $\theta_{23}^\nu = 45^\circ$, and $\mathcal{O}(1)$ charged-lepton coefficients $c_{12}^e = 0.8$, $c_{23}^e = 1.2$, $c_{13}^e = 0.8$, with aligned phases $\phi_{12}^e = \phi_{23}^e = 352^\circ$. Numerical diagonalization gives the PMNS magnitudes in Table I.

TABLE I. Numerical PMNS matrix (absolute values) for the representative NO-I benchmark described in the text.

$ U_{e1} $	$ U_{e2} $	$ U_{e3} $
0.83	0.54	0.15
$ U_{\mu 1} $	$ U_{\mu 2} $	$ U_{\mu 3} $
0.44	0.60	0.67
$ U_{\tau 1} $	$ U_{\tau 2} $	$ U_{\tau 3} $
0.35	0.59	0.73

The leptonic Jarlskog invariant is

$$J_{\text{CP}} = \text{Im}[U_{e1}U_{\mu 2}U_{e2}^*U_{\mu 1}^*] \simeq -0.031, \quad (36)$$

consistent with $J_{\text{CP}} \sim s_{12}c_{12}s_{23}c_{23}s_{13}c_{13}^2 \sin \delta$.

VII. NUFIT 6.0 COMPARISON

Using NuFIT 6.0 [9] (NO) central values, we compute illustrative pulls

$$\chi^2 = \sum_i \frac{(x_i - x_i^{\text{bf}})^2}{\sigma_i^2}. \quad (37)$$

The total $\chi^2 \simeq 0.6$ for this benchmark, confirming that the NO-I region of the coefficient scan is fully compatible with current data.

VIII. DISCRETE SYMMETRY AND ANOMALY CONSISTENCY

The lattice textures can be enforced by a discrete Z_N symmetry with $N = 18$ or 54 , consistent with the lattice interpretation. Assigning FN charges

$$Q(L_i) + Q(E_j^c) \equiv p_{ij}^e \pmod{N}, \quad (38)$$

the Yukawa operator

$$L_i H_d E_j^c \left(\frac{\phi}{M} \right)^{p_{ij}^e} \quad (39)$$

is invariant. Discrete gauge anomaly cancellation follows the Ibáñez–Ross conditions [30], which can be satisfied generation by generation for Z_{18} or Z_{54} with the above charge assignments.

IX. MAJORANA PHASES AND NEUTRINOLESS DOUBLE BETA DECAY

If neutrinos are Majorana, the PMNS matrix contains two additional physical phases beyond the Dirac phase. In the PDG convention one writes

$$U_{\text{PMNS}}^{(\text{PDG})} = \tilde{U}(\theta_{12}, \theta_{23}, \theta_{13}, \delta) \text{diag}\left(1, e^{i\alpha_{21}/2}, e^{i\alpha_{31}/2}\right), \quad (40)$$

where \tilde{U} carries the three mixing angles and Dirac phase δ , and $(\alpha_{21}, \alpha_{31})$ are the Majorana phases.

The neutrinoless double beta decay amplitude is controlled by the effective Majorana mass

$$m_{\beta\beta} \equiv \left| \sum_{i=1}^3 (U_{\text{PMNS}})_{ei}^2 m_i \right| \quad (41)$$

$$= \left| m_1 c_{12}^2 c_{13}^2 + m_2 s_{12}^2 c_{13}^2 e^{i\alpha_{21}} + m_3 s_{13}^2 e^{i(\alpha_{31} - 2\delta)} \right|,$$

with $s_{ij} \equiv \sin \theta_{ij}$, $c_{ij} \equiv \cos \theta_{ij}$.

A. Single- B scaling for $m_{\beta\beta}$ (normal ordering)

In our benchmark normal ordering scaling

$$m_3 : m_2 : m_1 \sim 1 : \epsilon : \epsilon^2, \quad (42)$$

and with $s_{13}^2 \sim \epsilon^2$ and $c_{13} \simeq 1$, the three contributions to Eq. (41) scale as

$$m_{\beta\beta} \sim \mathcal{O}(m_3) \times \max(c_{12}^2 \epsilon^2, s_{12}^2 \epsilon, \epsilon^2) \sim s_{12}^2 \epsilon m_3, \quad (43)$$

where the dominant term arises from the m_2 contribution modulated by $s_{12}^2 \simeq 0.30$. Thus, in the absence of tuned cancellations, the single- B framework predicts

$$m_{\beta\beta} \sim \frac{s_{12}^2 m_3}{B}. \quad (44)$$

B. Illustrative numerical range

Adopting a representative normal-ordering spectrum with $m_3 \simeq 50$ meV and $m_2 \simeq 8.6$ meV, the three terms in Eq. (41) evaluate to approximately 1.2, 2.7, and 1.1 meV respectively, giving

$$m_{\beta\beta} \sim 1\text{--}5 \text{ meV}, \quad (45)$$

where the spread reflects unknown Majorana phases in Eq. (41). This is below current experimental limits but within reach of next-generation experiments aiming at the few-meV regime [31].

TABLE II. Illustrative NuFIT 6.0 pulls (normal ordering) for the NO-I benchmark of Table I.

Observable	Model	Pull
$\sin^2 \theta_{12}$	0.298	-0.4σ
$\sin^2 \theta_{23}$	0.461	0.5σ
$\sin^2 \theta_{13}$	0.0221	0.1σ
δ	291°	0.3σ

X. PHENOMENOLOGY OF THE TWO NORMAL-ORDERING (NO) SOLUTIONS

Global fits to oscillation data (NuFIT 6.0 [9]) admit two normal-ordering (NO) solutions differing mainly in the atmospheric octant and the preferred value of the Dirac CP phase. In the single- B lattice framework, these two solutions correspond to distinct interference patterns between the neutrino and charged-lepton sectors in $U_{\text{PMNS}} = U_e^\dagger U_\nu$ [Eq. (5)].

A. NO-I: Lower-Octant Solution

In the first solution, $\theta_{23} < 45^\circ$ and the Dirac phase is in the range $\delta \sim 250^\circ\text{--}320^\circ$ (centered near 287°). In our framework this arises when the cancellation in

$$U_{e3} \simeq \theta_{13}^\nu - \theta_{12}^e \sin \theta_{23}^\nu e^{i\phi} \quad (46)$$

is moderate, so that $|U_{e3}| \sim \epsilon$ without strong fine tuning. Predictions:

- θ_{23} slightly below maximal due to constructive interference in the 23 block.
- δ in the third quadrant, displaced $\sim 15^\circ$ above 270° by $\mathcal{O}(\epsilon)$ corrections.
- $m_{\beta\beta} \simeq 3\text{--}4$ meV (for vanishing Majorana phases) and $|J_{\text{CP}}| \simeq 0.027$, essentially identical to NO-II (see Sec. XI).

B. NO-II: Upper-Octant Solution

In the second solution, $\theta_{23} > 45^\circ$ and δ shifts upward to $\sim 300^\circ$. This corresponds to a different relative phase ϕ between U_e and U_ν such that the interference in U_{e3} is stronger. Predictions:

- θ_{23} in the upper octant due to opposite-sign interference.
- δ displaced upward by $\mathcal{O}(15^\circ)$ relative to NO-I.
- $m_{\beta\beta}$ and $|J_{\text{CP}}|$ essentially unchanged from NO-I; the octant flip leaves these observables invariant (Table V).

C. Distinguishing Observables

The two solutions can be distinguished experimentally through:

1. Precision measurement of θ_{23} octant at DUNE [12]/Hyper-K [13]/IceCube [14], building on current constraints from Super-K [32], NOvA [33], and T2K [34]. T2K has provided some of the strongest existing constraints on δ and θ_{23} , including hints for $\delta \sim 270^\circ$ and some preference for the upper octant.
2. Improved determination of δ .
3. Combined fits of δ and θ_{23} correlations from DUNE, Hyper-K, IceCube [14], JUNO [15], and T2K.

Because J_{CP} and $m_{\beta\beta}$ are nearly identical between the two branches (Table V), neither $0\nu\beta\beta$ searches [31] nor CP-violation measurements alone can discriminate between NO-I and NO-II; the octant of θ_{23} and its correlated shift in δ remain the definitive discriminators. Table III collects the key properties of the two solutions.

Within the lattice-flavon framework, the two NO solutions therefore map onto distinct interference phases between U_e and U_ν , making the correlation between θ_{23} and δ a sharp test of the single- B organizing principle.

Table IV presents the Fritzsche–Xing rotation angles and phase obtained by fitting the FX decomposition to the PDG matrix for each branch. The charged-lepton angle $\theta_\ell \approx 12^\circ$ and the neutrino angle $\theta_\nu \approx 29^\circ\text{--}30^\circ$ are approximately invariant between the two solutions; the latter lies below the tribimaximal value $\theta_\nu^{\text{TBM}} \simeq 33.6^\circ$. In contrast, the atmospheric-sector angle θ shifts from 43.6° in NO-I to 46.4° in NO-II, while the FX phase ϕ_{FX} shifts by roughly -17° . Thus the familiar PDG octant ambiguity $\theta_{23} \leftrightarrow 90^\circ - \theta_{23}$ translates in the FX representation into a correlated $(\theta, \phi_{\text{FX}})$ ambiguity: the two branches differ by $\Delta\theta \approx +2.8^\circ$ and $\Delta\phi_{\text{FX}} \approx -17^\circ$, while the 12-sector angles that encode θ_{12} and θ_{13} are essentially unchanged. This structure reflects the fact that, in the FX factorization, the $R_{23}(\theta)$ rotation and the phase matrix P_ϕ jointly control both θ_{23} and δ , so a shift in one necessarily entails a compensating shift in the other.

D. Comparison with the quark-sector FX phase

In the quark sector, an FX-type fit to the CKM matrix yields $\phi_{\text{FX}}^{(\text{CKM})} \approx 90^\circ$ [6, 12, 16], i.e. maximal CP violation

TABLE III. Summary comparison of the two normal-ordering solutions. Values of θ_{23} and δ are the 2σ scan medians (used as FX benchmarks; see Table IV); J_{CP} and $m_{\beta\beta}$ are the 2σ branch means from Table V. The last column indicates whether the observable discriminates between the two solutions.

Observable	NO-I (LO)	NO-II (HO)	Discrim.?
θ_{23}	42.9°	45.8°	✓
δ	286°	304°	✓
θ_ℓ (FX)	12.4°	11.8°	weak
θ (FX)	43.6°	46.4°	✓
θ_ν (FX)	30.2°	28.4°	weak
ϕ_{FX}	-106°	-124°	✓
J_{CP}	-0.027	-0.025	×
$m_{\beta\beta}$ [meV]	3.3	3.6	×
Theory prior	favored	disfavored	—

TABLE IV. Fritzsche–Xing parameters fitted to the PDG mixing angles for the two normal-ordering branches. Common inputs: $\sin^2 \theta_{12} = 0.303$, $\sin^2 \theta_{13} = 0.0220$. The atmospheric angle and Dirac phase are taken from the 2σ scan medians in Table V. The FX parameterization is $U_{\text{PMNS}}^{(\text{FX})} = R_{12}^T(\theta_\ell) P_\phi R_{23}(\theta) R_{12}(\theta_\nu)$. The PDG θ_{23} octant ambiguity ($\sin^2 \theta_{23} \leftrightarrow 1 - \sin^2 \theta_{23}$, correlated with a shift in δ) maps in the FX representation to a correlated shift $(\theta, \phi_{\text{FX}}) \rightarrow (\theta + \Delta\theta, \phi_{\text{FX}} + \Delta\phi_{\text{FX}})$, with $\Delta\theta \approx +2.8^\circ$ and $\Delta\phi_{\text{FX}} \approx -17^\circ$, while the 12-sector angles θ_ℓ and θ_ν remain approximately invariant.

Parameter	NO-I (LO)	NO-II (HO)
$\sin^2 \theta_{23}$ (PDG)	0.463	0.514
δ (PDG)	286°	304°
θ_ℓ	12.4°	11.8°
θ	43.6°	46.4°
θ_ν	30.2°	28.4°
ϕ_{FX}	-106° (-0.59 π)	-124° (-0.69 π)
J_{CP}	-0.030	-0.025

given the angular prefactors. It is instructive to ask what the corresponding situation is in the lepton sector.

From Table IV, the leptonic FX phase is $\phi_{\text{FX}} \simeq -106^\circ$ (NO-I) and -124° (NO-II), departing from the quark-like value $\pm 90^\circ$ by roughly 16° and 34° , respectively. This departure has two correlated consequences:

1. *Submaximal leptonic CP violation.* Since $J_{\text{CP}} \propto \sin \phi_{\text{FX}}$, the suppression factor $|\sin \phi_{\text{FX}} / \sin 90^\circ|$ is 0.96 for NO-I and 0.83 for NO-II. The leptonic Jarlskog invariant is therefore reduced by 4%–17% relative to its angular bound.
2. *Departure of θ_ν from the tribimaximal value.* Constraining $\phi_{\text{FX}} = -90^\circ$ and refitting the three FX angles to the PDG matrix yields $\theta_\nu \simeq 33^\circ$, essentially the exact tribimaximal value $\theta_\nu^{\text{TBM}} = \arctan(1/\sqrt{2}) \simeq 33.6^\circ$. However, this constrained fit cannot simultaneously reproduce the observed reactor angle: $\sin^2 \theta_{13}$ comes out as 0.009 (NO-I) or 0.006 (NO-II), far below the measured 0.022. In the unconstrained fit, the additional freedom of ϕ_{FX} allows θ_{13} to be matched, but at the cost of pulling θ_ν down to $\sim 29^\circ$ – 30° .

Thus the “neat 90° ” of the quark-sector FX phase finds

no direct counterpart in the lepton sector. The non-trivial value of θ_{13} —ultimately traced to the charged-lepton correction $\theta_{12}^e \sim \epsilon^{17/9}$ —forces ϕ_{FX} away from $\pm 90^\circ$ and simultaneously pulls the neutrino 12-angle below its TBM value. This provides a concrete, parameterization-level encoding of a well-known qualitative fact: the observed reactor angle requires a departure from exact tribimaximal mixing that is absorbed partly by θ_ν and partly by the CP phase.

XI. PARAMETER SCAN AND ANALYTIC CORRELATIONS IN THE TWO-NO PICTURE

The mapping of the two normal-ordering solutions (NO-I and NO-II) to the lattice-flavon framework can be visualized by scanning the $\mathcal{O}(1)$ coefficients and relative phases entering the small charged-lepton rotations while keeping the neutrino-dominant angles near their best-fit values. We implement $U_{\text{PMNS}} = U_e^\dagger U_\nu$ with U_ν near the NO best fit and U_e built from the B -lattice power-counting angles $\theta_{12}^e \sim \epsilon^{17/9}$, $\theta_{23}^e \sim \epsilon^2$, $\theta_{13}^e \sim \epsilon^{20/9}$ multiplied by $\mathcal{O}(1)$ coefficients and including relative phases in the 12 and 13 charged-lepton rotations.

A. Phase alignment from the single-flavon structure

The scan assumes approximate alignment of the charged-lepton 12 and 23 rotation phases, $\phi_{12}^e \approx \phi_{23}^e$. This assumption follows from the single-flavon origin of all Yukawa entries combined with a numerical property of the lattice exponents.

In a Froggatt–Nielsen model with a single flavon Φ , each Yukawa entry arises from a messenger chain carrying p_{ij} powers of $\langle \Phi \rangle / \Lambda$. If the $\mathcal{O}(1)$ couplings at each messenger vertex are approximately real—so that CP violation originates dominantly from the complex phase $\phi_0 \equiv \arg \langle \Phi \rangle$ of the flavon VEV—then

$$Y_{ij} \simeq |c_{ij}| \epsilon^{p_{ij}} e^{i p_{ij} \phi_0}. \quad (47)$$

The left-handed rotation that enters U_e diagonalizes $Y_e Y_e^\dagger$. In the hierarchical limit the ij rotation angle is $\theta_{ij}^e \sim |Y_{ij}/Y_{jj}|$ with phase

$$\phi_{ij}^e = (p_{ij}^e - p_{jj}^e) \phi_0. \quad (48)$$

For the charged-lepton texture in Eq. (19) this gives

$$\phi_{12}^e = \frac{17}{9} \phi_0, \quad \phi_{23}^e = \frac{18}{9} \phi_0 = 2\phi_0, \quad (49)$$

so the misalignment is

$$\phi_{12}^e - \phi_{23}^e = -\frac{\phi_0}{9}. \quad (50)$$

The near-equality $p_{12}^e - p_{22}^e = \frac{17}{9} \approx 2 = p_{23}^e - p_{33}^e$ ensures that the two rotation phases are automatically aligned to within $\sim \phi_0/9$.

For a maximally CP-violating flavon VEV ($\phi_0 \sim \pi$) the misalignment is $|\phi_{12}^e - \phi_{23}^e| \simeq 20^\circ$; this motivates the alignment width $\sigma \simeq 20^\circ$ adopted in the scan below. Since $\phi_0 \equiv \arg \langle \Phi \rangle$ is the single source of CP violation in the model—all physical CP-violating phases are integer or rational multiples of ϕ_0 , and CP is conserved in the limit $\phi_0 \rightarrow 0$ (real VEV)—taking $\phi_0 \sim \pi$ represents the natural scale of an unsuppressed complex phase and yields the largest misalignment consistent with the single-flavon structure. Multiple messenger species or complex $\mathcal{O}(1)$ vertex couplings would scatter the phases around the single-source baseline, but by amounts of order $\phi_0/9$ per additional phase, preserving approximate alignment.

The 13 rotation phase, by contrast, satisfies $\phi_{13}^e = \frac{20}{9} \phi_0$, so $\phi_{13}^e - \phi_{23}^e = \frac{2}{9} \phi_0$ —a misalignment twice as large. For this reason the scan treats ϕ_{13}^e as an independent random variable.

B. Scan result: two branches in the (θ_{23}, δ) plane

Figure 2 displays the resulting distribution in the plane of the PDG Dirac phase δ versus the atmospheric angle θ_{23} . The lower- and upper-octant solutions appear

as two distinct branches, corresponding to different interference patterns between U_e and U_ν . The lower-octant branch is significantly more populated in the scan (roughly 4:1 over the upper octant), reflecting the fact that the near-maximal neutrino sector combined with the small charged-lepton correction $\theta_{23}^e \sim \epsilon^2 \approx 2^\circ$ generically leaves θ_{23} slightly below 45° ; pushing it into the upper octant requires the $\mathcal{O}(1)$ coefficients and phases to conspire somewhat. In this sense the framework carries a mild theoretical prior for NO-I. Current data do not yet resolve the ambiguity: NuFIT 6.0 finds local minima at both $\sin^2 \theta_{23} \approx 0.47$ and ≈ 0.56 with $\Delta\chi^2 < 4$ between them, and for normal ordering δ is essentially unconstrained [9], although T2K data hint at $\delta \sim 270^\circ$ with some preference for the upper octant [34]. Precision measurements of the θ_{23} octant at DUNE, Hyper-K, and IceCube [14] will therefore be decisive; the framework predicts that if θ_{23} is found in the upper octant, δ should be correspondingly shifted upward along the analytic correlation band.

Notably, while θ_{23} and δ differ markedly between the two branches, the Jarlskog invariant J_{CP} and the effective Majorana mass $m_{\beta\beta}$ are essentially branch-independent (Table V): both branches yield $J_{\text{CP}} \simeq -0.027$ and $m_{\beta\beta} \simeq 3\text{--}4$ meV (for vanishing Majorana phases), with distributions that overlap broadly. This near-degeneracy has two sources. First, the factor $s_{23}c_{23} = \frac{1}{2} \sin(2\theta_{23})$ in J_{CP} is stationary at maximal mixing and varies by less than 0.3% between $\theta_{23} = 42.9^\circ$ and 45.8° . Second, while $\sin \delta$ differs by $\sim 15\%$ between the branch medians, the broad scan dispersions ($\sigma_\delta \sim 34^\circ\text{--}43^\circ$) wash out much of this shift in the branch-averaged J_{CP} . Similarly, $m_{\beta\beta}$ is dominated by the m_2 term with coefficient $|U_{e2}|^2 \simeq s_{12}^2 c_{13}^2$, which is insensitive to the atmospheric octant. The discriminating observables between the two NO solutions are therefore θ_{23} and δ themselves, not J_{CP} or $m_{\beta\beta}$.

TABLE V. Branch-averaged predictions from the illustrative coefficient scan. We classify points by the atmospheric-octant branch (LO: $\theta_{23} < 45^\circ$, HO: $\theta_{23} > 45^\circ$). We apply NuFIT-style cuts on $\sin^2 \theta_{12}$ and $\sin^2 \theta_{13}$ at the indicated level; the “ 2σ ” band is implemented as a Gaussian proxy (twice the quoted 1σ widths), since the NuFIT δ and θ_{23} profiles are notably non-Gaussian for NO. The effective Majorana mass $m_{\beta\beta}$ uses the B -lattice spectrum ($m_1 = \epsilon^2 m_3 \simeq 1.8$ meV) with Majorana phases set to zero; varying the Majorana phases over their full range broadens $m_{\beta\beta}$ to the $\sim 1\text{--}5$ meV window of Eq. (45). Units: δ and θ_{23} are in degrees; $m_{\beta\beta}$ is in meV.

Cut & Branch	δ	θ_{23}	$m_{\beta\beta}$	J_{CP}
1σ LO ($N = 5082$)	286.3 ± 33.3	42.8 ± 1.3	3.30 ± 0.66	-0.0272 ± 0.0068
1σ HO ($N = 600$)	297.2 ± 47.2	45.7 ± 0.7	3.61 ± 0.74	-0.0246 ± 0.0082
2σ LO ($N = 18011$)	286.8 ± 33.6	42.8 ± 1.3	3.33 ± 0.67	-0.0271 ± 0.0069
2σ HO ($N = 3397$)	298.9 ± 42.8	46.1 ± 1.0	3.64 ± 0.74	-0.0250 ± 0.0084

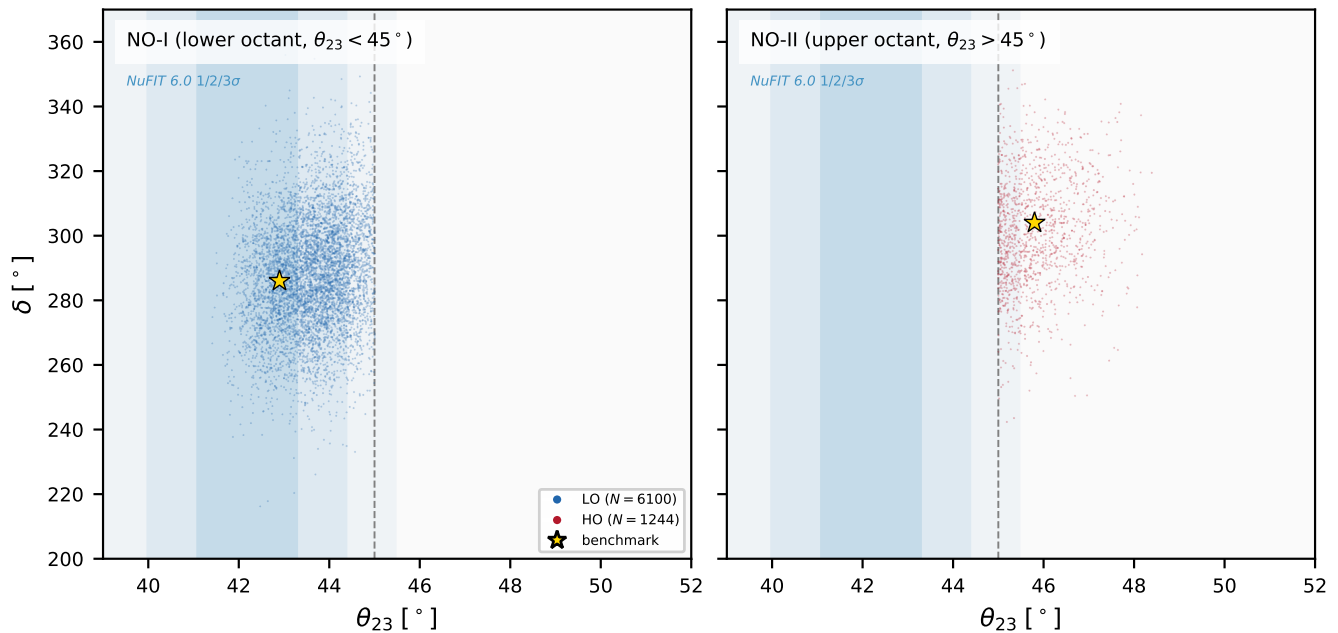


FIG. 2. Two-branch structure in the (θ_{23}, δ) plane from the $\mathcal{O}(1)$ coefficient scan. *Left*: NO-I (lower octant, $\theta_{23} < 45^\circ$); *Right*: NO-II (upper octant, $\theta_{23} > 45^\circ$). NuFIT 6.0 2σ cuts on $\sin^2 \theta_{12}$ and $\sin^2 \theta_{13}$ are applied; the NuFIT 6.0 (NO) 1σ – 3σ ranges for θ_{23} are indicated by the shaded bands. The star marks the benchmark of Table I. The lower octant is favored $\sim 4:1$ by point count.

C. Analytic correlation formulas: δ – θ_{23} linkage

Leading-order octant– δ theorem. To leading nontrivial order in the small charged-lepton angles, the two-branch structure in the (θ_{23}, δ) plane follows from a single complex interference parameter controlling U_{e3} . The full reactor element receives contributions from both the 12 and 13 charged-lepton rotations,

$$U_{e3} \simeq s_{13}^\nu e^{-i\delta_\nu} - \theta_{12}^e s_{23}^\nu e^{i\phi_{12}^e} - \theta_{13}^e c_{23}^\nu e^{i\phi_{13}^e}. \quad (51)$$

In the B -lattice textures the ratio of the two correction terms is $\theta_{13}^e c_{23}^\nu / (\theta_{12}^e s_{23}^\nu) = \epsilon^{1/3} \approx 0.57$, so the second correction is comparable in size, not parametrically small. Nevertheless, the dominant correlation structure is captured by retaining only the larger θ_{12}^e term. Define

$$r \equiv \frac{\theta_{12}^e s_{23}^\nu}{s_{13}^\nu}, \quad \Phi_e \equiv \phi_{12}^e - \delta_\nu, \quad (52)$$

so that the reactor element reduces to

$$U_{e3} \simeq s_{13}^\nu e^{-i\delta_\nu} (1 - r e^{-i\Phi_e}). \quad (53)$$

Writing $U_{e3} = s_{13} e^{-i\delta}$ immediately yields

$$\delta \simeq \delta_\nu - \arg(1 - r e^{-i\Phi_e}) \quad (54)$$

The observed Dirac phase δ is thus the neutrino-sector phase δ_ν shifted by a correction $\arg(1 - r e^{-i\Phi_e})$ that encodes the interference between the neutrino-dominant

reactor amplitude $s_{13}^\nu e^{-i\delta_\nu}$ and the charged-lepton correction $\theta_{12}^e s_{23}^\nu e^{i\phi_{12}^e}$. The magnitude and sign of this shift depend on two quantities: the ratio r , which measures the relative size of the two interfering amplitudes, and the effective phase difference $\Phi_e = \phi_{12}^e - \delta_\nu$, which controls the direction of the shift in the complex plane. For the B -lattice values $r \sim \mathcal{O}(1)$, the shift is typically $\sim 5^\circ$ – 15° , displacing δ from δ_ν into the range $\sim 280^\circ$ – 305° .

The atmospheric angle receives its dominant correction from the charged-lepton 23 rotation,

$$\theta_{23} \simeq \theta_{23}^\nu - \theta_{23}^e \cos \phi_{23}^e. \quad (55)$$

Thus the sign of $(\theta_{23} - \theta_{23}^\nu)$ is controlled by the same charged-lepton phase that enters U_{e3} .

Correlated branch structure. As shown in Sec. XI A, the single-flavon origin of the B -lattice textures ensures $\phi_{12}^e \approx \phi_{23}^e$ to within $\sim \phi_0/9$. Under this alignment, the sign of the octant shift ($\theta_{23} - 45^\circ$) correlates directly with the direction of the phase displacement ($\delta - \delta_\nu$). Lower- and upper-octant solutions therefore correspond to opposite signs of the interference term in Eq. (54), producing two distinct branches in the (θ_{23}, δ) plane.

Regime of validity. Equations (54) and (55) retain the dominant charged-lepton corrections but neglect the $\theta_{13}^e c_{23}^\nu$ term in Eq. (51), which is $\sim \epsilon^{1/3} \approx 57\%$ of the retained $\theta_{12}^e s_{23}^\nu$ term. The analytic formulas should therefore be understood as capturing the *qualitative correlation structure*—the existence of two branches and the sign of the octant– δ linkage—rather than as precision

predictions of $\delta(\theta_{23})$. Numerical scans, which include all three charged-lepton rotations and their relative phases, confirm that the two-branch structure and the predictive octant– δ linkage are robust (Fig. 2).

The essential result is structural: the same interference that fixes $|U_{e3}|$ determines both the magnitude and the direction of the Dirac-phase shift and simultaneously selects the atmospheric octant.

Figure 3 collects the full set of mixing angles and CP phases, providing a compact visual comparison of the two normal-ordering branches and the hierarchy of charged-lepton corrections.

XII. CONCLUSIONS

We have extended the single-flavon B -lattice framework to the lepton sector. The construction rests on two ingredients: (i) B -lattice power counting ($\epsilon = 1/B$), which fixes charged-lepton Yukawa suppressions and neutrino mass eigenvalue ratios, and (ii) an approximate mu–tau symmetry ($Z_2^{\mu\tau}$ [21–23], A_4 [25, 35], or S_4 [24, 36]), which fixes the $\mathcal{O}(1)$ structure of the neutrino 23 block. The charged-lepton sector requires only ingredient (i); the neutrino sector requires both.

The central result is a two-branch prediction in the (θ_{23}, δ) plane:

- **NO-I** (lower octant): $\theta_{23} \approx 43^\circ$, $\delta \approx 286^\circ$, favored by a $\sim 4:1$ theoretical prior;
- **NO-II** (upper octant): $\theta_{23} \approx 46^\circ$, $\delta \approx 304^\circ$.

The two branches arise because the same charged-lepton–neutrino interference that generates the reactor element U_{e3} also controls the direction of the Dirac-phase shift; the single-flavon origin of the Yukawa textures ensures the required phase alignment between the 12 and 23 charged-lepton rotations to within $\sim \phi_0/9$. This correlation is stable under $\mathcal{O}(1)$ coefficient variations.

Three observables are nearly branch-independent and therefore cannot discriminate: $J_{\text{CP}} \simeq -0.027$, $m_{\beta\beta} \simeq 3\text{--}4$ meV (for vanishing Majorana phases), and $\sin^2 \theta_{13} \simeq 0.022$. The discriminating observables are θ_{23} and δ themselves.

The framework makes a falsifiable prediction: if future data establish the upper octant, δ must lie near 300° ; if the lower octant, near 285° . Discovery of δ in the first or second quadrant ($0^\circ\text{--}180^\circ$) in either octant would rule out the single- B lattice textures with aligned phases. The decisive measurements are $\nu_\mu \rightarrow \nu_e$ appearance rates and their CP conjugates at DUNE [12] and Hyper-Kamiokande [13], which are directly sensitive to $\sin \delta$ through the Jarlskog interference term, combined with octant determination from ν_μ disappearance and atmospheric neutrino samples at IceCube [14]. Independent resolution of the mass ordering by JUNO [15] eliminates the $\delta \leftrightarrow (\pi - \delta)$ degeneracy from matter effects. Together these measurements, building on current constraints from Super-Kamiokande [32], NOvA [33], and

T2K [34], will provide a direct test of this organizing principle across quarks and leptons.

Appendix A: Analytic PMNS matrix in terms of model parameters

We collect here the explicit construction of the PMNS matrix used throughout this paper.

1. Model parameters

The framework has two sectors, each specified by a small number of parameters.

a. Neutrino sector (4 parameters). The neutrino diagonalization matrix U_ν is parameterized in the PDG convention,

$$U_\nu = R_{23}(\theta_{23}^\nu) R_{13}(\theta_{13}^\nu, \delta_\nu) R_{12}(\theta_{12}^\nu), \quad (\text{A1})$$

with $\theta_{23}^\nu \simeq 45^\circ$ (near-maximal, from mu–tau symmetry), $\theta_{12}^\nu \simeq 35^\circ$ (near-tribimaximal), $\theta_{13}^\nu \sim \epsilon \simeq 0.15$ rad (from $\mathcal{O}(\epsilon)$ mu–tau breaking), and $\delta_\nu \sim 290^\circ$ (neutrino CP phase).

b. Charged-lepton sector (6 parameters). The charged-lepton diagonalization matrix U_e is built from three small rotations with phases,

$$U_e = R_{23}(\theta_{23}^e, \phi_{23}^e) R_{13}(\theta_{13}^e, \phi_{13}^e) R_{12}(\theta_{12}^e, \phi_{12}^e), \quad (\text{A2})$$

where the rotation angles are fixed by the B -lattice exponent differences up to $\mathcal{O}(1)$ coefficients:

$$\theta_{12}^e = c_{12}^e \epsilon^{17/9}, \quad \theta_{23}^e = c_{23}^e \epsilon^2, \quad \theta_{13}^e = c_{13}^e \epsilon^{20/9}, \quad (\text{A3})$$

with $c_{ij}^e = \mathcal{O}(1)$. The phases ϕ_{ij}^e arise from the complex flavon VEV as described in Sec. XI A; the single-flavon structure enforces the approximate alignment $\phi_{12}^e \approx \phi_{23}^e$ with misalignment $\sim \phi_0/9$.

c. Numerical base values. With $\epsilon = 1/B \simeq 0.1867$:

$$\begin{aligned} \theta_{12}^e|_{c=1} &= \epsilon^{17/9} \simeq 0.042 \text{ rad} \simeq 2.4^\circ, \\ \theta_{23}^e|_{c=1} &= \epsilon^2 \simeq 0.035 \text{ rad} \simeq 2.0^\circ, \\ \theta_{13}^e|_{c=1} &= \epsilon^{20/9} \simeq 0.024 \text{ rad} \simeq 1.4^\circ. \end{aligned} \quad (\text{A4})$$

2. Rotation matrix conventions

Each rotation $R_{ij}(\theta, \phi)$ acts in the ij plane with a phase ϕ attached to the off-diagonal sine entries. Explicitly,

$$R_{12}(\theta, \phi) = \begin{pmatrix} c & s e^{i\phi} & 0 \\ -s e^{-i\phi} & c & 0 \\ 0 & 0 & 1 \end{pmatrix}, \quad (\text{A5})$$

Summary of Mixing Angles and Phases in the Lattice-Flavon Lepton Model

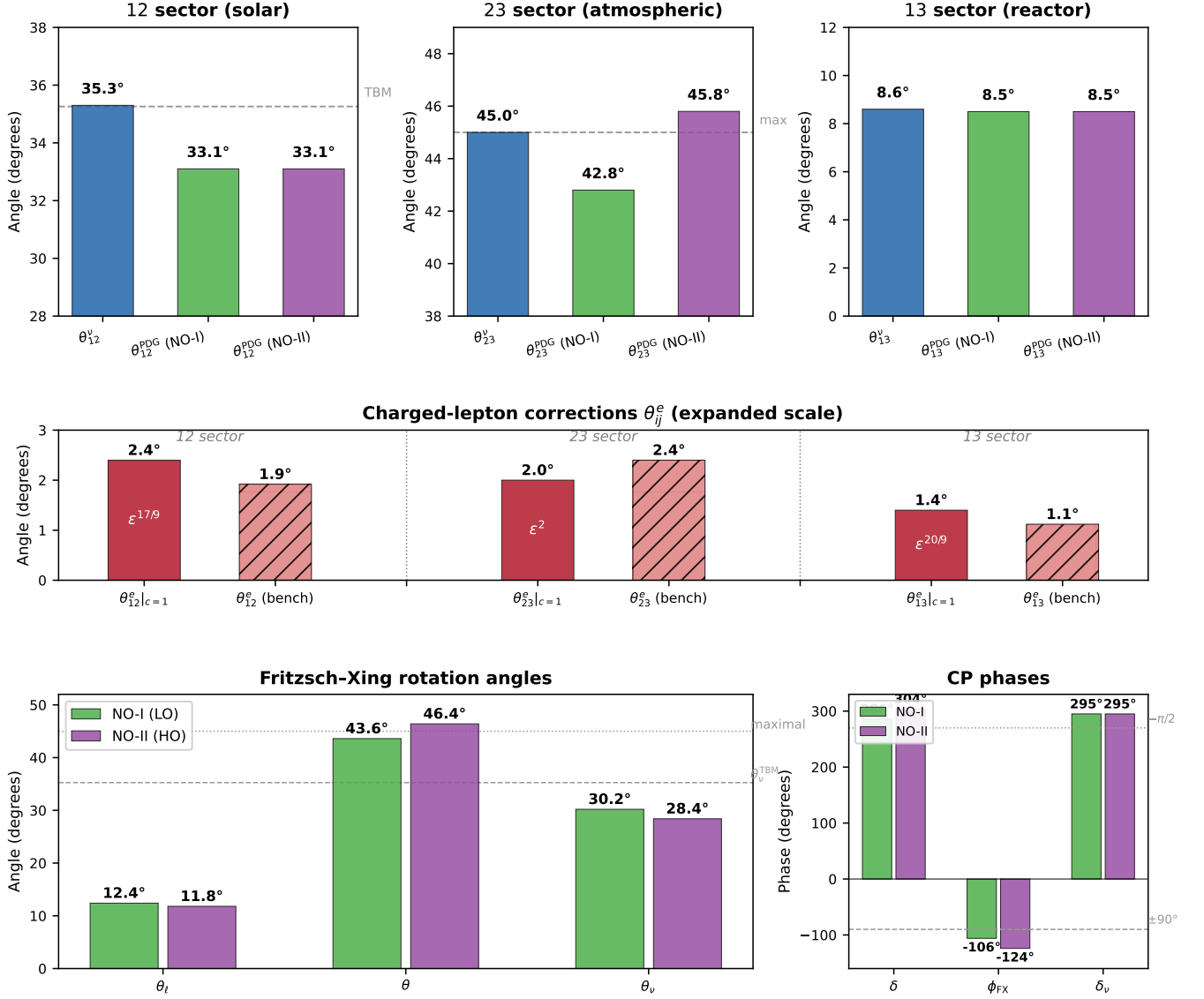


FIG. 3. Summary of mixing angles and phases in the lattice-flavon lepton model. *Top row*: PDG mixing angles θ_{12} , θ_{23} , θ_{13} compared with the neutrino-sector values (θ_{12}^y , θ_{23}^y , θ_{13}^y) for the two normal-ordering branches (NO-I and NO-II); dashed lines mark the tribimaximal and maximal reference values. *Middle row*: charged-lepton correction angles θ_{ij}^e at the B -lattice base scale ($c = 1$, solid bars) and at the benchmark values (hatched bars), on an expanded vertical scale; labels indicate the ϵ -power scaling. *Bottom left*: Fritsch–Xing rotation angles (θ_ℓ , θ , θ_ν) for NO-I (green) and NO-II (purple), with tribimaximal and maximal reference lines. *Bottom right*: Dirac phase δ , FX phase ϕ_{FX} , and neutrino-sector phase δ_ν for both branches; the dashed line marks the quark-sector reference $\pm 90^\circ$.

$$R_{13}(\theta, \phi) = \begin{pmatrix} c & 0 & s e^{i\phi} \\ 0 & 1 & 0 \\ -s e^{-i\phi} & 0 & c \end{pmatrix}, \quad (\text{A6})$$

$$R_{23}(\theta, \phi) = \begin{pmatrix} 1 & 0 & 0 \\ 0 & c & s e^{i\phi} \\ 0 & -s e^{-i\phi} & c \end{pmatrix}, \quad (\text{A7})$$

where $c \equiv \cos \theta$, $s \equiv \sin \theta$. When the phase argument is omitted, $\phi = 0$.

3. Leading-order PMNS matrix

Since all charged-lepton angles satisfy $\theta_{ij}^e \ll 1$, U_e may be expanded to first order:

$$U_e \simeq \mathcal{K} + \begin{pmatrix} 0 & \theta_{12}^e e^{i\phi_{12}^e} & \theta_{13}^e e^{i\phi_{13}^e} \\ -\theta_{12}^e e^{-i\phi_{12}^e} & 0 & \theta_{23}^e e^{i\phi_{23}^e} \\ -\theta_{13}^e e^{-i\phi_{13}^e} & -\theta_{23}^e e^{-i\phi_{23}^e} & 0 \end{pmatrix} + \mathcal{O}(\epsilon^{34/9}). \quad (\text{A8})$$

The Hermitian conjugate is

$$U_e^\dagger \simeq \mathcal{K} + \begin{pmatrix} 0 & -\theta_{12}^e e^{i\phi_{12}^e} & -\theta_{13}^e e^{i\phi_{13}^e} \\ \theta_{12}^e e^{-i\phi_{12}^e} & 0 & -\theta_{23}^e e^{i\phi_{23}^e} \\ \theta_{13}^e e^{-i\phi_{13}^e} & \theta_{23}^e e^{-i\phi_{23}^e} & 0 \end{pmatrix}. \quad (\text{A9})$$

The PMNS matrix $U_{\text{PMNS}} = U_e^\dagger U_\nu$ then takes the form

$$(U_{\text{PMNS}})_{\alpha i} = (U_\nu)_{\alpha i} + \sum_{\beta \neq \alpha} (\Delta_e^\dagger)_{\alpha\beta} (U_\nu)_{\beta i} + \mathcal{O}(\epsilon^{34/9}), \quad (\text{A10})$$

where $\Delta_e^\dagger \equiv U_e^\dagger - \mathcal{K}$ is the off-diagonal perturbation in Eq. (A9).

4. Explicit PMNS elements

Using the shorthand $(U_\nu)_{\alpha i} \equiv U_{\alpha i}^\nu$ and suppressing the superscript e on the charged-lepton angles and phases, the nine elements are:

$$U_{e1} = U_{e1}^\nu - \theta_{12} e^{i\phi_{12}} U_{\mu 1}^\nu - \theta_{13} e^{i\phi_{13}} U_{\tau 1}^\nu, \quad (\text{A11})$$

$$U_{e2} = U_{e2}^\nu - \theta_{12} e^{i\phi_{12}} U_{\mu 2}^\nu - \theta_{13} e^{i\phi_{13}} U_{\tau 2}^\nu, \quad (\text{A12})$$

$$\begin{aligned} U_{e3} &= U_{e3}^\nu - \theta_{12} e^{i\phi_{12}} U_{\mu 3}^\nu - \theta_{13} e^{i\phi_{13}} U_{\tau 3}^\nu \\ &= s_{13}^\nu e^{-i\delta_\nu} - \theta_{12} s_{23}^\nu c_{13}^\nu e^{i\phi_{12}} \\ &\quad - \theta_{13} c_{23}^\nu c_{13}^\nu e^{i\phi_{13}}, \end{aligned} \quad (\text{A13})$$

$$U_{\mu 1} = U_{\mu 1}^\nu + \theta_{12} e^{-i\phi_{12}} U_{e1}^\nu - \theta_{23} e^{i\phi_{23}} U_{\tau 1}^\nu, \quad (\text{A14})$$

$$U_{\mu 2} = U_{\mu 2}^\nu + \theta_{12} e^{-i\phi_{12}} U_{e2}^\nu - \theta_{23} e^{i\phi_{23}} U_{\tau 2}^\nu, \quad (\text{A15})$$

$$\begin{aligned} U_{\mu 3} &= U_{\mu 3}^\nu + \theta_{12} e^{-i\phi_{12}} U_{e3}^\nu - \theta_{23} e^{i\phi_{23}} U_{\tau 3}^\nu \\ &= s_{23}^\nu c_{13}^\nu + \theta_{12} s_{13}^\nu e^{-i(\phi_{12} + \delta_\nu)} \\ &\quad - \theta_{23} c_{23}^\nu c_{13}^\nu e^{i\phi_{23}}, \end{aligned} \quad (\text{A16})$$

$$U_{\tau 1} = U_{\tau 1}^\nu + \theta_{13} e^{-i\phi_{13}} U_{e1}^\nu + \theta_{23} e^{-i\phi_{23}} U_{\mu 1}^\nu, \quad (\text{A17})$$

$$U_{\tau 2} = U_{\tau 2}^\nu + \theta_{13} e^{-i\phi_{13}} U_{e2}^\nu + \theta_{23} e^{-i\phi_{23}} U_{\mu 2}^\nu, \quad (\text{A18})$$

$$\begin{aligned} U_{\tau 3} &= U_{\tau 3}^\nu + \theta_{13} e^{-i\phi_{13}} U_{e3}^\nu + \theta_{23} e^{-i\phi_{23}} U_{\mu 3}^\nu \\ &= c_{23}^\nu c_{13}^\nu + \theta_{13} s_{13}^\nu e^{-i(\phi_{13} + \delta_\nu)} \\ &\quad + \theta_{23} s_{23}^\nu c_{13}^\nu e^{-i\phi_{23}}. \end{aligned} \quad (\text{A19})$$

In Eqs. (A13), (A16), and (A19) we have substituted the explicit PDG forms of the third-column neutrino elements ($U_{e3}^\nu = s_{13}^\nu e^{-i\delta_\nu}$, $U_{\mu 3}^\nu = s_{23}^\nu c_{13}^\nu$, $U_{\tau 3}^\nu = c_{23}^\nu c_{13}^\nu$).

5. PDG observables to leading order

The standard PDG extraction gives, to leading order in θ_{ij}^e :

$$\sin^2 \theta_{13} = |U_{e3}|^2, \quad (\text{A20})$$

$$\sin^2 \theta_{12} = \frac{|U_{e2}|^2}{1 - |U_{e3}|^2}, \quad (\text{A21})$$

$$\begin{aligned} \sin^2 \theta_{23} &= \frac{|U_{\mu 3}|^2}{1 - |U_{e3}|^2} \\ &\simeq s_{23}^{\nu 2} - 2 s_{23}^\nu c_{23}^\nu \theta_{23} \cos \phi_{23}, \end{aligned} \quad (\text{A22})$$

where in the last line we used Eq. (A16) and $c_{13}^\nu \simeq 1$ since $\theta_{13}^\nu \sim \epsilon$. Equation (A22) is equivalent to the atmospheric-angle correction Eq. (55) in the main text.

The Dirac CP phase is extracted from the Jarlskog invariant,

$$J_{\text{CP}} = \text{Im}[U_{e1} U_{\mu 2} U_{e2}^* U_{\mu 1}^*], \quad (\text{A23})$$

together with the relation $J_{\text{CP}} = c_{12} s_{12} c_{23} s_{23} c_{13}^2 s_{13} \sin \delta$. The reactor element Eq. (A13) directly yields the analytic δ -theorem of Eq. (54) upon writing $U_{e3} = s_{13} e^{-i\delta}$.

6. Summary of model-parameter counting

The full PMNS matrix depends on 10 continuous parameters: 4 neutrino ($\theta_{12}^\nu, \theta_{23}^\nu, \theta_{13}^\nu, \delta_\nu$) and 6 charged-lepton ($c_{12}^e, c_{23}^e, c_{13}^e, \phi_{12}^e, \phi_{23}^e, \phi_{13}^e$). Of these, the B -lattice and mu-tau symmetry fix:

- $\theta_{23}^\nu \simeq 45^\circ$ and $\theta_{12}^\nu \simeq \arctan(1/\sqrt{2}) \simeq 35.3^\circ$ (mu-tau / TBM structure);
- $\theta_{13}^\nu \sim \epsilon$ (one free $\mathcal{O}(1)$ parameter);
- the power-law scalings in Eq. (A3) (three free $\mathcal{O}(1)$ coefficients);
- $\phi_{12}^e \approx \phi_{23}^e$ with misalignment $\sim \phi_0/9$ (single-flavon phase alignment).

In the scan of Sec. XI, δ_ν and ϕ_{13}^e are the only unconstrained phases; ϕ_{12}^e and ϕ_{23}^e are drawn from a narrow Gaussian about a common value, and the three $\mathcal{O}(1)$ coefficients are varied uniformly in $[0.5, 1.5]$.

Appendix B: Relation to the companion-paper neutrino texture

The companion paper [5] derives a neutrino exponent matrix from the strict Weinberg-operator additive rule

$p_{ij}^\nu = Q(L_i) + Q(L_j)$ with lepton-doublet charges $Q(L_i) = (1, \frac{1}{2}, 0)$, giving

$$p_{\text{comp}}^\nu = \begin{pmatrix} 2 & \frac{3}{2} & 1 \\ \frac{3}{2} & 1 & \frac{1}{2} \\ 1 & \frac{1}{2} & 0 \end{pmatrix}. \quad (\text{B1})$$

This hierarchical texture reproduces the correct mass eigenvalue scaling $m_1 : m_2 : m_3 \sim \epsilon^2 : \epsilon : 1$, which is the only neutrino observable the companion paper addresses. The present paper adopts instead the flat texture of Eq. (28), in which $p_{L_2}^\nu = p_{L_3}^\nu = 0$, so that the entire 23 block is $\mathcal{O}(m_0)$. This flattening is necessary to accommodate the large atmospheric and solar mixing angles through an approximate mu–tau symmetry in the $\mathcal{O}(1)$ coefficients. The mass eigenvalue hierarchy is preserved: it arises from the $\mathcal{O}(\epsilon)$ suppression of the first-generation couplings rather than from a hierarchical 23 block.

The two assignments share common features: (i) the same expansion parameter $\epsilon = 1/B$; (ii) the same first-generation suppression $p_{ij}^\nu \geq 1$; (iii) identical mass-eigenvalue ratios $m_1 : m_2 : m_3 \sim \epsilon^2 : \epsilon : 1$; and (iv) iden-

tical charged-lepton mass scaling $m_e : m_\mu : m_\tau \propto \epsilon^{29/6} : \epsilon^{5/3} : 1$. They differ only in the 23 sub-block of the neutrino texture—precisely the sector where the additional mu–tau symmetry input of the present paper acts. In this sense the two treatments are complementary: the companion paper establishes the B -lattice mass framework, while the present paper introduces the symmetry structure required for the PMNS mixing pattern.

In earlier two-over-two constructions the Majorana nature of the neutrino operator required a charge normalization denominator of 18, reflecting the bilinear structure of the effective dimension-five operator. In the present effective-texture formulation this doubling is absorbed into the definition of p_{ij}^ν , allowing a minimal denominator of 9 without altering the predicted B -scaling relations for masses or mixing.

ACKNOWLEDGMENTS

VB gratefully acknowledges support from the William F. Vilas Estate.

-
- [1] C. D. Froggatt and H. B. Nielsen, “Hierarchy of quark masses, Cabibbo angles and CP violation,” Nucl. Phys. B **147**, 277 (1979).
- [2] M. Leurer, Y. Nir, and N. Seiberg, “Mass matrix models,” Nucl. Phys. B **398**, 319 (1993), arXiv:hep-ph/9212278.
- [3] M. Leurer, Y. Nir, and N. Seiberg, “Mass matrix models: The sequel,” Nucl. Phys. B **420**, 468 (1994), arXiv:hep-ph/9310320.
- [4] V. Barger, “One-flavon flavor: A single hierarchical parameter B organizes quarks and leptons at M_Z ,” Phys. Rev. D **113**, 013002 (2026), arXiv:2512.13630 [hep-ph].
- [5] V. Barger, “Two-over-Two Lattice Flavor from a Single Flavon with Three Messenger Chains,” Phys. Rev. D (2026), in press, arXiv:2602.18393 [hep-ph].
- [6] V. Barger, “Quark Mixing from a Lattice Flavon Model: A Four-Magnitude Parameterization,” submitted to Phys. Rev. D (2026), arXiv:2603.00810 [hep-ph].
- [7] N. Cabibbo, “Unitary symmetry and leptonic decays,” Phys. Rev. Lett. **10**, 531 (1963).
- [8] M. Kobayashi and T. Maskawa, “CP-violation in the renormalizable theory of weak interaction,” Prog. Theor. Phys. **49**, 652 (1973).
- [9] I. Esteban, M. C. Gonzalez-Garcia, M. Maltoni, I. Martinez-Soler, J. P. Pinheiro, and T. Schwetz, “NuFit-6.0: Updated global analysis of three-flavor neutrino oscillations,” JHEP **12**, 216 (2024), arXiv:2410.05380 [hep-ph]; see also <https://www.nu-fit.org>.
- [10] B. Pontecorvo, “Mesonium and antimesonium,” Zh. Eksp. Teor. Fiz. **33**, 549 (1957) [Sov. Phys. JETP **6**, 429 (1958)].
- [11] Z. Maki, M. Nakagawa, and S. Sakata, “Remarks on the unified model of elementary particles,” Prog. Theor. Phys. **28**, 870 (1962).
- [12] B. Abi *et al.* (DUNE Collaboration), “Deep Underground Neutrino Experiment (DUNE), Far Detector Technical Design Report, Volume II: DUNE Physics,” arXiv:2002.03005 [hep-ex] (2020).
- [13] K. Abe *et al.* (Hyper-Kamiokande Collaboration), “Hyper-Kamiokande Design Report,” arXiv:1805.04163 [physics.ins-det] (2018).
- [14] R. Abbasi *et al.* (IceCube Collaboration), “Measurement of atmospheric neutrino mixing with improved IceCube DeepCore calibration and data processing,” Phys. Rev. D **108**, 012014 (2023), arXiv:2304.12236 [hep-ex].
- [15] A. Abusleme *et al.* (JUNO Collaboration), “JUNO physics and detector,” Prog. Part. Nucl. Phys. **123**, 103927 (2022), arXiv:2104.02565 [hep-ex].
- [16] H. Fritzsch and Z.-z. Xing, “On the parametrization of flavor mixing in the standard model,” Phys. Rev. D **57**, 594 (1998), arXiv:hep-ph/9708366.
- [17] C. Jarlskog, “Commutator of the quark mass matrices in the standard electroweak model and a measure of maximal CP nonconservation,” Phys. Rev. Lett. **55**, 1039 (1985).
- [18] S. Navas *et al.* (Particle Data Group), “Review of particle physics,” Phys. Rev. D **110**, 030001 (2024).
- [19] P. F. Harrison, D. H. Perkins, and W. G. Scott, “Tribimaximal mixing and the neutrino oscillation data,” Phys. Lett. B **530**, 167 (2002), arXiv:hep-ph/0202074.
- [20] S. Weinberg, “Baryon- and lepton-nonconserving processes,” Phys. Rev. Lett. **43**, 1566 (1979).
- [21] P. F. Harrison and W. G. Scott, “ μ – τ reflection symmetry in lepton mixing and neutrino oscillations,” Phys. Lett. B **547**, 219 (2002), arXiv:hep-ph/0210197.
- [22] C. S. Lam, “Symmetry of lepton mixing,” Phys. Lett. B **656**, 193 (2007), arXiv:0708.3665 [hep-ph].
- [23] Z.-z. Xing and Z.-h. Zhao, “A review of μ – τ symmetry in

- neutrino physics,” *Rep. Prog. Phys.* **79**, 076201 (2016), arXiv:1512.04207 [hep-ph].
- [24] S. F. King and C. Luhn, “Neutrino mass and mixing with discrete symmetry,” *Rep. Prog. Phys.* **76**, 056201 (2013), arXiv:1301.1340 [hep-ph].
- [25] E. Ma and G. Rajasekaran, “Softly broken A_4 symmetry for nearly degenerate neutrino masses,” *Phys. Rev. D* **64**, 113012 (2001), arXiv:hep-ph/0106291.
- [26] P. Minkowski, “ $\mu \rightarrow e\gamma$ at a rate of one out of 10^9 muon decays?,” *Phys. Lett. B* **67**, 421 (1977).
- [27] T. Yanagida, “Horizontal symmetry and masses of neutrinos,” in *Proceedings of the Workshop on Unified Theory and Baryon Number of the Universe*, eds. O. Sawada and A. Sugamoto (KEK, 1979), p. 95.
- [28] M. Gell-Mann, P. Ramond, and R. Slansky, “Complex spinors and unified theories,” in *Supergravity*, eds. P. van Nieuwenhuizen and D. Freedman (North-Holland, 1979), p. 315, arXiv:1306.4669 [hep-th].
- [29] R. N. Mohapatra and G. Senjanović, “Neutrino mass and spontaneous parity nonconservation,” *Phys. Rev. Lett.* **44**, 912 (1980).
- [30] L. E. Ibáñez and G. G. Ross, “Discrete gauge symmetries and the origin of baryon and lepton number conservation in supersymmetric versions of the standard model,” *Phys. Lett. B* **260**, 256 (1991).
- [31] M. Agostini, G. Benato, J. A. Detwiler, J. Menéndez, and F. Vissani, “Toward the discovery of matter creation with neutrinoless double-beta decay,” *Rev. Mod. Phys.* **95**, 025002 (2023), arXiv:2202.01787 [hep-ex].
- [32] M. Abe *et al.* (Super-Kamiokande Collaboration), “Atmospheric neutrino oscillation analysis with improved event reconstruction in Super-Kamiokande IV,” *Phys. Rev. D* **109**, 072014 (2024), arXiv:2311.05105 [hep-ex].
- [33] M. A. Acero *et al.* (NOvA Collaboration), “Improved measurement of neutrino oscillation parameters by the NOvA experiment,” *Phys. Rev. D* **106**, 032004 (2022), arXiv:2108.08219 [hep-ex].
- [34] K. Abe *et al.* (T2K Collaboration), “Measurements of neutrino oscillation parameters from the T2K experiment using 3.6×10^{21} protons on target,” *Eur. Phys. J. C* **83**, 782 (2023), arXiv:2303.03222 [hep-ex].
- [35] G. Altarelli and F. Feruglio, “Tri-bimaximal neutrino mixing, A_4 , and the modular symmetry,” *Nucl. Phys. B* **741**, 215 (2006), arXiv:hep-ph/0512103.
- [36] H. Ishimori, T. Kobayashi, H. Ohki, Y. Shimizu, H. Okada, and M. Tanimoto, “Non-Abelian discrete symmetries in particle physics,” *Prog. Theor. Phys. Suppl.* **183**, 1 (2010), arXiv:1003.3552 [hep-th].